The Astrophysical Journal Letters, 762:L18 (6pp), 2013 January 10 doi:10.1088/2041-8205/762/2/L18

COMPACT BINARY PROGENITORS OF SHORT GAMMA-RAY BURSTS

Bruno Giacomazzo[1], Rosalba Perna[2], Luciano Rezzolla[3], Eleonora Troja[4,5], and Davide Lazzati[6]
[1] JILA, University of Colorado and National Institute of Standards and Technology, Boulder, CO 80309, USA
[2] JILA and Department of Astrophysical and Planetary Sciences, University of Colorado, Boulder, CO 80309, USA
[3] Max-Planck-Institut für Gravitationsphysik, Albert-Einstein-Institut, Potsdam D-14476, Germany
[4] NASA Goddard Space Flight Center, Greenbelt, MD 20771, USA
[5] Department of Astronomy, University of Maryland, College Park, MD 20742, USA
[6] Department of Physics, NC State University, 2401 Stinson Drive, Raleigh, NC 27695-8202, USA
Received 2012 October 30; accepted 2012 November 27; published 2012 December 13

ABSTRACT

In recent years, detailed observations and accurate numerical simulations have provided support to the idea that mergers of compact binaries containing either two neutron stars (NSs) or an NS and a black hole (BH) may constitute the central engine of short gamma-ray bursts (SGRBs). The merger of such compact binaries is expected to lead to the production of a spinning BH surrounded by an accreting torus. Several mechanisms can extract energy from this system and power the SGRBs. Here we connect observations and numerical simulations of compact binary mergers, and use the current sample of SGRBs with measured energies to constrain the mass of their powering tori. By comparing the masses of the tori with the results of fully general-relativistic simulations, we are able to infer the properties of the binary progenitors that yield SGRBs. By assuming a constant efficiency in converting torus mass into jet energy, $\epsilon_{\rm jet} = 10\%$, we find that most of the tori have masses smaller than $0.01\,M_{\odot}$, favoring "high-mass" binary NSs mergers, i.e., binaries with total masses $\gtrsim$1.5 the maximum mass of an isolated NS. This has important consequences for the gravitational wave signals that may be detected in association with SGRBs, since "high-mass" systems do not form a long-lived hypermassive NS after the merger. While NS–BH systems cannot be excluded to be the engine of at least some of the SGRBs, the BH would need to have an initial spin of $\sim$0.9 or higher.

Key words: accretion, accretion disks – gamma-ray burst: general – gravitational waves – methods: numerical – stars: neutron

Online-only material: color figures

1. INTRODUCTION

Binary neutron star (BNS) and neutron star–black hole (NS–BH) binaries are the leading candidates for the central engine of short gamma-ray bursts (SGRBs; Blinnikov et al. 1984; Paczynski 1986; Eichler et al. 1989). They are also one of the most powerful sources of gravitational waves (GWs), and advanced interferometric detectors are expected to observe these sources at rates of $\sim$0.4–400 and $\sim$0.2–300 events per year for BNS and NS–BH, respectively (Abadie et al. 2010).

Fully general-relativistic simulations have shown how such mergers can lead to the formation of accretion disks around spinning BHs (Baiotti et al. 2008; Etienne et al. 2009; Kiuchi et al. 2009; Faber & Rasio 2012). Moreover, when magnetic fields are present, they can provide one of the mechanisms necessary to extract energy, and power collimated relativistic jets (Rezzolla et al. 2011; Etienne et al. 2012).

So far, properties of the progenitors of SGRBs have been inferred by studying their redshift distribution, close environment, host galaxy types (Bloom et al. 2006; Zhang et al. 2009; Berger 2011), and by comparing those observations with predictions from population synthesis models (Perna & Belczynski 2002; Belczynski et al. 2006; O'Shaughnessy et al. 2008). In this Letter we make a connection between theory and observations, which allows us to directly probe the SGRB progenitors. In particular, we consider a complete (to date) sample of SGRBs with measured redshifts, and link the properties of their observed emissions to the masses of the tori responsible for their generation. By comparing these tori with the theoretical predictions of Rezzolla et al. (2010) and of Foucart (2012), we are able to infer the properties of the compact binaries that may have generated such bursts.

In Section 2 we provide details on the sample of SGRBs considered in this Letter. In Section 3, we use the theoretical results to compute the masses of the tori that have generated such bursts, and link them to their progenitors. In Section 4 we show how GWs may be used to further constrain the progenitors, and in Section 5 we summarize our main results.

2. GRB SAMPLE DATA

We selected our sample of SGRBs based on three criteria: duration, hardness ratio, and spectral lags. *Swift* SGRBs with known redshift are listed in Table 1. SGRBs with a temporally extended emission (EE) were also considered. In the latter case, the quoted energetics include the contribution of the short–hard spike, and of the EE. Since the two emission episodes typically have a comparable energy budget (Norris et al. 2011), the presence of EE affects our calculations by a factor $\approx$2.

The burst energetics, $E_{\gamma,\rm iso}$ (Column 3 in Table 1), were calculated by using the prompt emission spectral parameters (mainly from Sakamoto et al. 2011 and Goldstein et al. 2012) and shifted to a common rest-frame energy band (Bloom et al. 2001). When possible, we used measurements of the broadband GRB spectrum (e.g., by the *Fermi*/GBM) and calculated $E_{\gamma,\rm iso}$ in the comoving 10 keV–10 MeV energy range. In most cases, only *Swift*/BAT observations are available, and we report the burst energetics in the narrower 15–150 keV rest-frame band, thus unavoidably underestimating the bolometric energy release. For a typical Band spectrum (Band et al. 1993), peaking at $\approx$500 keV (Nava et al. 2011), we estimate an average k-correction factor of $\approx$6. We therefore do not expect that the uncertainty in the GRB spectral shape of *Swift* bursts may have a major impact on the results.

Table 1
SGRB Sample

GRB Name	z	$E_{\gamma,\rm iso}$ (erg)	ΔE (keV)	$M_{\rm torus}$ ($M_\odot$)
050509B	0.225	9.1×10^{47}	15–150	1.0×10^{-5}
050709(EE)	0.161	3.4×10^{49}	10–10^4	3.8×10^{-4}
050724(EE)	0.257	1.9×10^{50}	15–150	2.1×10^{-3}
051221A	0.546	2.9×10^{51}	10–10^4	3.3×10^{-2}
061006(EE)	0.438	2.1×10^{51}	10–10^4	2.4×10^{-2}
070429B	0.902	2.1×10^{50}	15–150	2.3×10^{-3}
070714B(EE)	0.923	1.6×10^{52}	10–10^4	1.8×10^{-1}
071227(EE)	0.381	1.2×10^{51}	10–10^4	1.4×10^{-2}
080905A	0.122	4.5×10^{49}	10–10^4	5.1×10^{-4}
090510	0.903	4.7×10^{52}	10–10^4	5.2×10^{-1}
100117A	0.920	1.4×10^{51}	10–10^4	1.6×10^{-2}
111117A	1.3	5.3×10^{51}	10–10^4	6.0×10^{-2}
051210	1.3	4.0×10^{50}	15–150	4.5×10^{-3}
060801	1.130	1.9×10^{50}	15–150	2.1×10^{-3}
061210(EE)	0.410	5.6×10^{50}	15–150	6.2×10^{-3}
070724A	0.457	2.3×10^{49}	15–150	2.5×10^{-4}
070729	0.8	1.6×10^{50}	15–150	1.8×10^{-3}
080123(EE)	0.495	5.7×10^{50}	15–150	6.3×10^{-3}
101219A	0.718	7.4×10^{51}	10–10^4	8.2×10^{-2}
060502B	0.287	9.8×10^{48}	15–150	1.1×10^{-4}
061217	0.827	6.8×10^{49}	15–150	7.6×10^{-4}
061201	0.111	9.4×10^{48}	15–150	1.1×10^{-4}
070809	0.473	7.9×10^{49}	15–150	8.8×10^{-4}
090515	0.403	1.0×10^{49}	15–150	1.2×10^{-4}

Notes. The different columns refer, respectively, to the GRB name, the redshift z derived from the GRB host, the isotropic equivalent gamma-ray energy $E_{\gamma,\rm iso}$, measured in the rest-frame energy band ΔE, and the mass of the torus $M_{\rm torus}$ (see Equation (1)). The different blocks refer to the uncertainty in the SGRB/host galaxy association (Bloom et al. 2002). The top one includes SGRBs with a precise identification of a host galaxy; those in the middle have a less certain association with their host; those in the bottom are significantly offset from the associated host galaxy, and are affected by a larger uncertainty.

Table 1 shows that SGRBs display a wide range of energies, from 10^{48} erg to 10^{52} erg, with a median value of 2×10^{50} erg. The quoted values refer to the isotropic equivalent gamma-ray energy, while the true energy scale also depends on the outflow beaming factor $f_b \equiv 1 - \cos(\theta_{\rm jet})$, being $\theta_{\rm jet}$ the jet opening angle. The degree of collimation of SGRBs is still a poorly constrained quantity, inferred values range from $f_b \approx 0.001$ to $f_b \approx 0.1$ (Burrows et al. 2006; Nicuesa Guelbenzu et al. 2012), but in most cases only weak lower bounds can be placed. Here, we use the isotropic energies listed in Table 1 to set an upper limit to the burst-energy release.

Assuming that all the SGRBs in our sample were produced by accretion tori around spinning BHs, we now correlate the values for the isotropic energy listed in Table 1 with the mass of such tori. In particular the torus mass is determined as

$$E_{\gamma,\rm iso} = \epsilon M_{\rm torus} c^2 \,, \qquad (1)$$

where ϵ is the efficiency in converting the mass of the torus $M_{\rm torus}$ into the isotropic gamma-ray emission $E_{\gamma,\rm iso}$. Here, ϵ is given by the product of two efficiencies: one to convert mass of the torus into jet energy, $\epsilon_{\rm jet}$, and the other to convert the latter into gamma rays, ϵ_γ.

Fully general-relativistic simulations of BNS mergers have shown the formation of thin and highly magnetized tori around spinning BHs (Rezzolla et al. 2010, 2011). Here we make the important assumption that SGRBs are powered via magnetic fields (Blandford & Znajek 1977; Blandford & Payne 1982; Tchekhovskoy et al. 2012) and ignore the effects of viscosity and neutrino cooling (Chen & Beloborodov 2007).[7] General-relativistic magnetohydrodynamic (GRMHD) simulations of accretion disks showed that the efficiency in converting torus mass and BH spin into jet energy (i.e., $\epsilon_{\rm jet}$) varies between a few percent up to more than 100% for maximally spinning BHs (De Villiers et al. 2005; Tchekhovskoy et al. 2011; McKinney et al. 2012; Fragile et al. 2012). The efficiency depends sensitively on the BH spin, the disk thickness, and the magnetic flux. Accounting for all of these effects is currently not possible, and thus we made the simplifying assumption of a constant efficiency for all BNS and NS–BH mergers, $\epsilon_{\rm jet} = 10\%$. While an obvious approximation, our main results do not change sensitively if $\epsilon_{\rm jet}$ is taken to be larger than $\sim$0.1%.

After the jet is emitted, a fraction of its energy is converted into gamma rays. The conversion efficiency for a sample of long and short *Swift* GRBs was computed by Zhang et al. (2007) by comparing the gamma-ray fluence with the brightness of the X-ray afterglow at early and late times. They find that, while the efficiency in long GRBs varies strongly from burst to burst, ranging from a fraction of a percent to almost 100%, in SGRBs the range is narrower, varying between 30% and 60%, with an average of 49%. We hence assume a fiducial value of $\epsilon_\gamma = 50\%$, so that the total efficiency in Equation (1) becomes $\epsilon = 5\%$. The last column of Table 1 shows the corresponding torus masses.

3. TORUS MASSES

In the following, we link $M_{\rm torus}$ to the theoretical predictions of Rezzolla et al. (2010) and of Foucart (2012), who derived analytic fits from the results of fully general-relativistic simulations of BNS and NS–BH mergers, respectively (see also Pannarale et al. 2011).

3.1. Binary Neutron Star Mergers

Rezzolla et al. (2010) derived a phenomenological expression to compute the masses of the tori formed by BNS mergers. Here we have revised that fit and expressed it as a function of two dimensionless quantities: the gravitational mass ratio $q \leqslant 1$ and the ratio between the gravitational mass of the binary and the maximum gravitational mass for an isolated NS ($M_{\rm BNS}/M_{\rm max}$). We derived

$$M_{\rm torus} = [c_1(1-q) + c_2][c_3(1+q) - M_{\rm BNS}/M_{\rm max}] \,. \qquad (2)$$

The coefficients $c_1 = 2.974 \pm 3.366$, $c_2 = 0.11851 \pm 0.07192$, and $c_3 = 1.1193 \pm 0.1579$ were determined by fitting Equation (2) to the results of the fully general-relativistic simulations of Baiotti et al. (2008) and Rezzolla et al. (2010), but rescaled to allow for a value of $M_{\rm max} = 2.20\,M_\odot$ to be more consistent with current observations of NS masses (see also Table 2).

The left panel of Figure 1 shows $M_{\rm torus}$ computed using Equation (2) as a function of q and $M_{\rm BNS}/M_{\rm max}$, while each of the red dotted lines represents the isocontour relative to an observed GRB in Table 1 when assuming our fiducial value $\epsilon = 5\%$. The right panel shows the distribution of torus masses obtained from observations (horizontal bars, see Table 1) together with the mass of the torus computed from numerical simulations of equal-mass BNSs ($q = 1$, see Table 2). As one

[7] For a discussion of neutrino-powered SGRBs and the relation between simulations and observations, see Lee et al. (2005), Oechslin & Janka (2006), and Fan & Wei (2011).

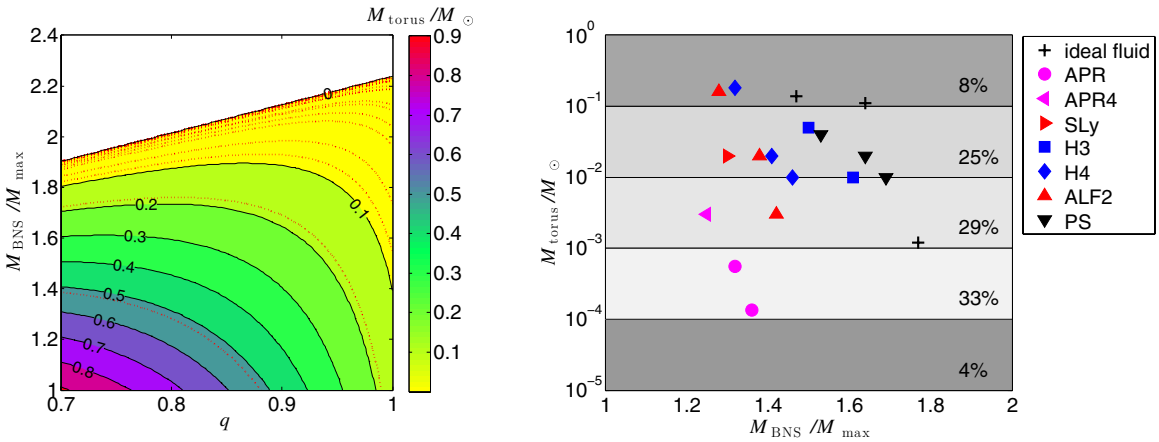

Figure 1. Left panel: $M_{\rm torus}/M_\odot$ as a function of the mass ratio q and of the ratio between the gravitational mass of the binary and the maximum mass for an isolated NS ($M_{\rm BNS}/M_{\rm max}$). $M_{\rm torus}$ has been computed using Equation (2). The dotted lines are the isocontours corresponding to the $M_{\rm torus}$ values in Table 1. Right panel: plot of $M_{\rm torus}$ as a function of $M_{\rm BNS}/M_{\rm max}$ for all the equal-mass ($q = 1$) simulations reported in Table 2. The horizontal bars give the percentage of the SGRBs in Table 1 that are generated by tori with that range of masses (assuming a total efficiency ϵ of 5% as in Table 1). Since the mass of the torus increases for $q < 1$, each point should be considered as a lower limit on the mass that can be obtained for that EOS and mass of the binary. The different points refer to $M_{\rm torus}$ computed from simulations of BNS mergers using different EOSs (see Table 2).

(A color version of this figure is available in the online journal.)

Table 2
BNS Simulations and Torus Masses

Model	$M_{\rm BNS}$ ($M_\odot$)	q	$M_{\rm torus}$ ($M_\odot$)	$M_{\rm max}$ ($M_\odot$)	$M_{\rm BNS}/M_{\rm max}$
1.46-45-IF	3.24	1.00	0.1374	2.20	1.47
1.62-45-IF	3.61	1.00	0.1101	2.20	1.64
M3.6q1.00	3.90	1.00	0.0012	2.20	1.77
M3.7q0.94	4.03	0.94	0.0121	2.20	1.83
M3.4q0.91	3.76	0.92	0.1202	2.20	1.71
M3.4q0.80	3.72	0.81	0.2524	2.20	1.69
M3.5q0.75	3.80	0.77	0.1939	2.20	1.73
M3.4q0.70	3.71	0.72	0.2558	2.20	1.69
APR145145	2.87	1.00	0.000549	2.18	1.32
APR1515	2.97	1.00	0.000134	2.18	1.36
APR1316	2.87	0.81	0.0275	2.18	1.32
APR135165	2.97	0.82	0.00707	2.18	1.36
APR4-28	2.77	1.00	0.003	2.21	1.25
SLy-27	2.67	1.00	0.02	2.05	1.30
H3-27	2.68	1.00	0.05	1.79	1.50
H3-29	2.87	1.00	0.01	1.79	1.61
H4-27	2.68	1.00	0.18	2.03	1.32
H4-29	2.87	1.00	0.02	2.03	1.41
H4-30	2.97	1.00	0.01	2.03	1.46
ALF2-27	2.67	1.00	0.16	2.09	1.28
ALF2-29	2.87	1.00	0.02	2.09	1.38
ALF2-30	2.97	1.00	0.003	2.09	1.42
PS-27	2.68	1.00	0.04	1.76	1.53
PS-29	2.88	1.00	0.02	1.76	1.64
PS-30	2.97	1.00	0.01	1.76	1.69

Notes. The different columns represent, respectively, the name of the model, the gravitational mass of the binary, $M_{\rm BNS}$, the mass ratio of the gravitational masses of the two NSs, q, the baryonic mass of the torus, $M_{\rm torus}$, the maximum gravitational mass of an isolated NS for the equation of state (EOS) used in that simulation, $M_{\rm max}$, and the ratio between the mass of the binary and $M_{\rm max}$, $M_{\rm BNS}/M_{\rm max}$. The different blocks of the table refer, from top to bottom, to the simulations by Baiotti et al. (2008), Rezzolla et al. (2010), Kiuchi et al. (2009), and Hotokezaka et al. (2011). Note that the simulations reported in Baiotti et al. (2008) and Rezzolla et al. (2010) used an ideal-fluid EOS and hence they can be scaled to different masses. Here we have chosen the values for an ideal-fluid EOS so that $M_{\rm max} = 2.20$, in agreement with current observations (Demorest et al. 2010).

can easily see, two-thirds of the SGRBs of our sample appear to be generated by tori with masses smaller than $\sim 10^{-2}\, M_\odot$. Moreover, since $M_{\rm torus}$ increases for $q < 1$, each point should be considered as a lower limit on the mass that can be obtained for that equation of state (EOS) and BNS mass. This means that while the energetics of most SGRBs can be explained by current numerical simulations, some of the less energetic SGRBs should result from BNS mergers with masses larger than the ones simulated so far (since $M_{\rm torus}$ decreases with increasing $M_{\rm BNS}$).

It is evident from the left panel of Figure 1 that for an ideal-fluid EOS, almost all of the SGRBs would be generated by BNSs with $M_{\rm BNS}/M_{\rm max} > 1.8$ and hence they would be "high-mass" systems. This means that the mass of the system would be too high to lead to the formation of a long-lived hypermassive NS (HMNS) and that the merger would produce a prompt collapse to BH. This is also true for the models with realistic EOSs shown in the right panel of Figure 1. For example, the two circles refer to simulations of equal-mass binaries using an APR EOS (models APR145145 and APR1515; see Kiuchi et al. 2009) and they produce tori with masses in the range of $\sim$33% of all SGRBs in our sample. As reported in Kiuchi et al. (2009), in both cases, collapse to BH occurs $\sim$1 ms after merger. We recall that the threshold $M_{\rm BNS}/M_{\rm max}$ below which a long-lived HMNS is formed is strongly dependent on the EOS. All the simulations that produce tori with masses $\lesssim 0.1\, M_\odot$ in the right panel of Figure 1 produce an HMNS that collapses on a timescale of few ms (Kiuchi et al. 2009; Rezzolla et al. 2010; Hotokezaka et al. 2011).[8] As we discuss in Section 4, this has a fundamental impact on the GW signal we may expect from SGRBs.

3.2. NS–BH Mergers

Foucart (2012) derived the following fit for the mass of the torus produced by an NS–BH merger:

$$M_{\rm torus} = \left(\frac{M_{\rm NS}^b}{M_{\rm NS}}\right) \left[\alpha (3/q)^{1/3} (1 - 2C_{\rm NS}) M_{\rm NS} - \beta R_{\rm isco} C_{\rm NS}\right], \quad (3)$$

[8] If ϵ was one order of magnitude smaller, $M_{\rm torus}$ would be 10 times larger, but 67% of the SGRBs would still have $M_{\rm torus} < 0.1\, M_\odot$ and hence be generated by "high-mass" systems.

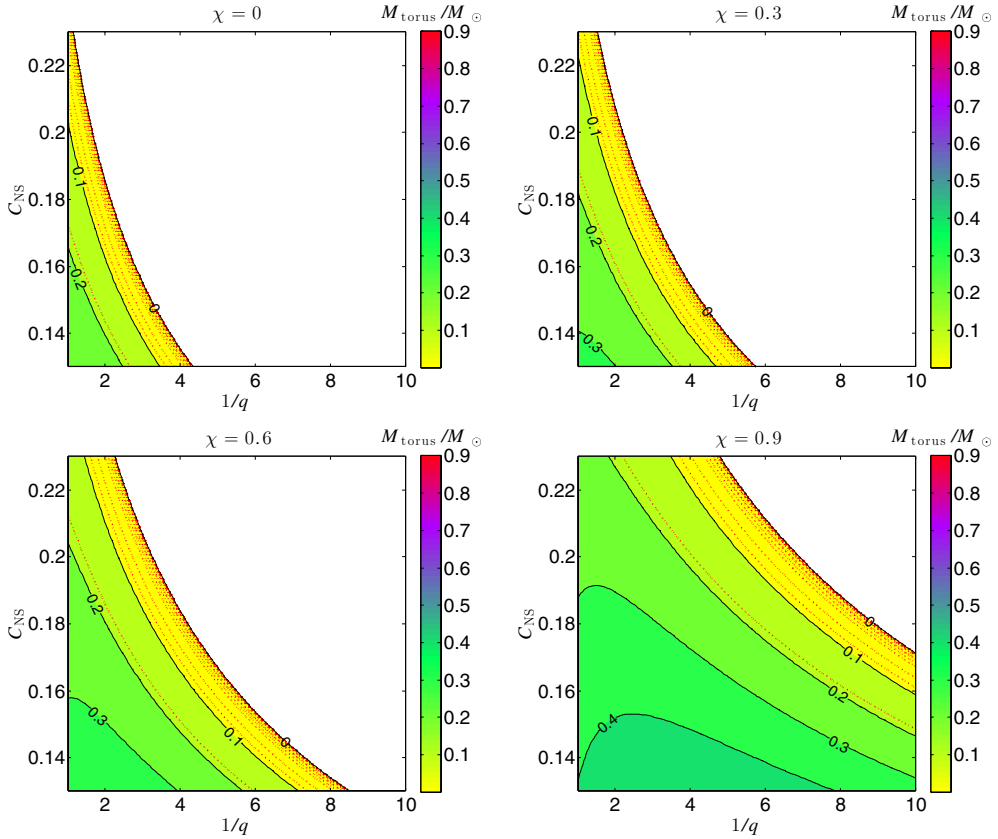

Figure 2. Similar to the left panel of Figure 1, but for the NS–BH case. $M_{\rm torus}$ is shown as a function of the NS compactness $C_{\rm NS}$ and mass ratio $1/q \equiv M_{\rm BH}/M_{\rm NS}$. $M_{\rm torus}$ is computed using Equation (3). Each panel assumes a different value for the dimensionless spin of the BH, χ. In all cases, we assume $M_{\rm NS} = 1.4\,M_\odot$. The dotted lines are the isocontours corresponding to the $M_{\rm torus}$ values in Table 1.

(A color version of this figure is available in the online journal.)

where $\alpha = 0.288 \pm 0.011$, $\beta = 0.148 \pm 0.007$, $M_{\rm NS}$ is the gravitational mass of the NS, $M^b_{\rm NS}$ its baryonic mass, $C_{\rm NS}$ the NS compactness, $1/q \equiv M_{\rm BH}/M_{\rm NS} > 1$ the ratio between the BH and NS masses, and $R_{\rm isco}$ the radius of the innermost stable circular orbit (Foucart 2012). We note that in order to compute $M_{\rm torus}$ we need to know the ratio $M_{\rm NS}/M^b_{\rm NS}$, for which there is no analytic expression available. Here we make the reasonable assumption that the baryonic mass is 10% larger than the gravitational mass.[9] This assumption may lead to a few percent error on the mass of the torus, which is sufficiently small to not affect the results of this Letter.

The four panels in Figure 2 show $M_{\rm torus}$, computed using Equation (3), as a function of the NS compactness $C_{\rm NS}$ and mass ratio $1/q$. Each panel assumes a different value for the dimensionless spin of the BH, χ. It is evident from this figure that not even the most rapidly spinning BH ($\chi = 0.9$) can explain the most energetic burst in our sample (GRB090510 with $M_{\rm torus} \sim 0.5\,M_\odot$). Moreover, if we account for the results of populations synthesis calculations (Belczynski et al. 2008), which predict most of the NS–BH binaries to have mass ratios $1/q$ between ∼7 and ∼10, while the NS compactness is expected to be larger than ∼0.16 (Steiner et al. 2012), then most of the SGRBs in our sample can be only explained if the binary has a BH with an initial spin of ∼0.9 or larger. From current observations of SGRBs, it is then clear that, while current simulations of BNS mergers may easily produce tori in the range required to explain all the current observations, NS–BH mergers cannot be used to explain the most energetic bursts.

4. CONSTRAINTS USING FUTURE GW OBSERVATIONS

As shown in Baiotti et al. (2008) and Rezzolla et al. (2010), the GW signal is strongly affected by the mass of the system and how close this is to the maximum mass for each particular EOS. BNSs with masses close to the maximum mass exhibit a prompt collapse to BH after the merger, while lower-mass systems produce an HMNS that can survive from few ms up to hundreds of ms (Baiotti et al. 2008; Rezzolla et al. 2010; Giacomazzo et al. 2011). GW signals from "high-mass" systems are simply composed of the inspiral, merger, and BH ring-down phases. Lower-mass systems instead display a more complex GW signal with a rich spectrum due to the emission of GWs from the HMNS formed after the merger. Such emission is important since it can help infer the properties of the NS EOS (Bauswein et al. 2012). However, since the GW signal emitted by the HMNS is in a range of frequencies between ∼2 kHz and ∼4 kHz (Baiotti et al. 2008; Bauswein et al. 2012), it may be difficult for advanced LIGO/Virgo to detect it, and a third generation of detectors, such as the Einstein Telescope, would be required (Andersson et al. 2011). On the other hand, the formation of an HMNS after the merger can also be inferred by measuring the delay time between the BNS merger (indicated by the GW signal) and the time of the emission of the SGRB (which we may assume coincident with BH formation). A delay

[9] For the NSs reported in Table 2, the baryonic mass $M^b_{\rm NS}$ is ∼8% larger than the gravitational mass $M_{\rm NS}$ for the ideal-fluid EOS and ∼11% larger for the APR EOS.

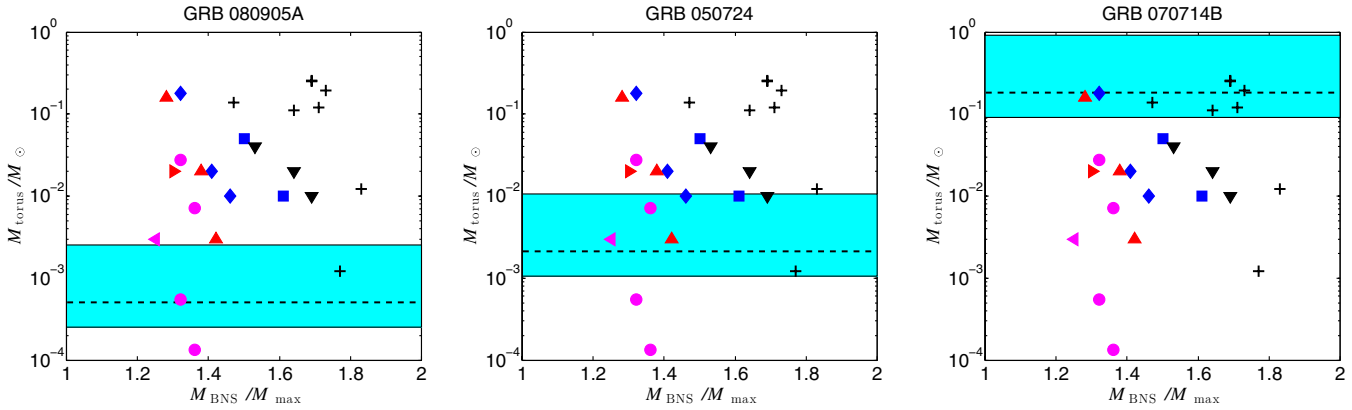

Figure 3. Different panels plot $M_{\rm torus}$ as a function of $M_{\rm BNS}/M_{\rm max}$ for all the simulations reported in Table 2, and compare them with three SGRBs taken from Table 1: GRB080905A, GRB050724, and GRB070714B. In each panel, a horizontal dashed line represents the value of $M_{\rm torus}$ reported in Table 1 while the shaded region represents the range of $M_{\rm torus}$ assuming a total efficiency between $\epsilon = 1\%$ and $\epsilon = 10\%$. Symbols for the various EOS from Table 2 are the same as in Figure 1, but here the $q \neq 1$ simulations have also been included.

(A color version of this figure is available in the online journal.)

time of ∼100 ms or larger would clearly indicate the formation of an HMNS.

As discussed in Section 3.1, we find that only the most energetic SGRBs can be compatible with a low-mass binary and hence the formation of an HMNS. For the greatest majority of SGRBs, a high-mass system is the most likely scenario, and hence we expect SGRBs to be observed simultaneously with GWs which would lack the high-frequency emission typical of the HMNS. Although the GW signal from a prompt collapse is not as rich as that from an HMNS, the simultaneous detection of an SGRB with the associated GW may help considerably in constraining the NS EOS.

This is illustrated in Figure 3 with a selection of three SGRBs from our sample (with low, medium, and high energetics). In each panel, the horizontal dashed line represents the value of $M_{\rm torus}$ reported in Table 1, while the shaded region represents the range of $M_{\rm torus}$ assuming a total efficiency ϵ between 1% and 10%. The various points represent $M_{\rm torus}$ computed from simulations of BNS mergers using different EOSs (see Table 2). If an SGRB was detected together with a GW signal, we could use the energetic of the burst to determine the torus mass (horizontal bars in Figure 3), while the GW signal could be used to infer the mass of the BNSs (which would give a vertical bar in those panels). The combination of these two pieces of information would restrict the allowed EOS parameter space.

In the case of NS–BH binaries, the mass ratio q and the spin of the BH can in principle be measured via GW observations; then a simultaneous detection of a GW and an SGRB would allow to set an independent constraint on the NS compactness $C_{\rm NS}$ and hence infer the NS EOS.

5. SUMMARY

We have performed a novel analysis of the energetics of SGRBs in connection with the properties of the compact binary systems that may have generated them. We have shown that most of the SGRBs could be produced by magnetized tori with masses lower than $\sim 0.01\ M_\odot$. Combining this information with the results of numerical simulations of NS–NS and NS–BH mergers, we have concluded that most of the SGRBs are consistent with the merger of "high-mass" BNS systems, i.e., with $M_{\rm BNS}/M_{\rm max} \gtrsim 1.5$. While NS–BH systems cannot be completely excluded, the BH would need to have an initial spin of ∼0.9, or higher. Moreover, the most energetic SGRBs, such as GRB090510, could not be produced by the merger of an NS with a BH.[10] We note that while our results are affected by some uncertainty in the exact value of the efficiency ϵ, our conclusions are robust as long as $\epsilon_{\rm jet} \gtrsim 0.1\%$ (i.e., $\epsilon \gtrsim 5 \times 10^{-4}$), which is much lower than what was observed in GRMHD simulations of jets from accretion disks (De Villiers et al. 2005; Tchekhovskoy et al. 2011; McKinney et al. 2012; Fragile et al. 2012).

GW signals from SGRBs would help validate our results. In particular, in the case of BNSs, since we find that SGRBs are most likely generated by "high-mass" BNSs, the GW signal would lack the features that are associated with the formation of an HMNS, since "high-mass" BNSs produce a prompt collapse to BH a few ms after merger. A simultaneous detection of GWs with SGRBs would help constrain the EOS of NS matter.

We thank J. M. Demopoulos, H.-T. Janka, and S. T. McWilliams for useful comments. B.G. and R.P. acknowledge support from NSF Grant No. AST 1009396 and NASA Grant No. NNX12AO67G. L.R. acknowledges support from the DFG grant SFB/Transregio 7 and by "CompStar," a Research Networking Programme of the ESF.

REFERENCES

Abadie, J., Abbott, B. P., Abbott, R., et al. 2010, CQGra, 27, 173001
Andersson, N., Ferrari, V., Jones, D. I., et al. 2011, GReGr, 43, 409
Baiotti, L., Giacomazzo, B., & Rezzolla, L. 2008, PhRvD, 78, 084033
Band, D., Matteson, J., Ford, L., et al. 1993, ApJ, 413, 281
Bauswein, A., Janka, H.-T., Hebeler, K., & Schwenk, A. 2012, PhRvD, 86, 063001
Belczynski, K., Perna, R., Bulik, T., et al. 2006, ApJ, 648, 1110
Belczynski, K., Taam, R. E., Rantsiou, E., & van der Sluys, M. 2008, ApJ, 682, 474
Berger, E. 2011, NewAR, 55, 1
Blandford, R. D., & Payne, D. G. 1982, MNRAS, 199, 883
Blandford, R. D., & Znajek, R. L. 1977, MNRAS, 179, 433
Blinnikov, S. I., Novikov, I. D., Perevodchikova, T. V., & Polnarev, A. G. 1984, SvAL, 10, 177
Bloom, J. S., Frail, D. A., & Sari, R. 2001, AJ, 121, 2879
Bloom, J. S., Kulkarni, S. R., & Djorgovski, S. G. 2002, AJ, 123, 1111
Bloom, J. S., Prochaska, J. X., Pooley, D., et al. 2006, ApJ, 638, 354
Burrows, D. N., Grupe, D., Capalbi, M., et al. 2006, ApJ, 653, 468

[10] See McWilliams & Levin (2011) for an alternative.

Chen, W.-X., & Beloborodov, A. M. 2007, ApJ, 657, 383
Demorest, P. B., Pennucci, T., Ransom, S. M., Roberts, M. S. E., & Hessels, J. W. T. 2010, Natur, 467, 1081
De Villiers, J.-P., Hawley, J. F., Krolik, J. H., & Hirose, S. 2005, ApJ, 620, 878
Eichler, D., Livio, M., Piran, T., & Schramm, D. N. 1989, Natur, 340, 126
Etienne, Z. B., Liu, Y. T., Shapiro, S. L., & Baumgarte, T. W. 2009, PhRvD, 79, 044024
Etienne, Z. B., Paschalidis, V., & Shapiro, S. L. 2012, PhRvD, 86, 084026
Faber, J. A., & Rasio, F. A. 2012, LRR, 15, 8
Fan, Y.-Z., & Wei, D.-M. 2011, ApJ, 739, 47
Foucart, F. 2012, PhRvD, 86, 124007
Fragile, P. C., Wilson, J., & Rodriguez, M. 2012, MNRAS, 424, 524
Giacomazzo, B., Rezzolla, L., & Baiotti, L. 2011, PhRvD, 83, 044014
Goldstein, A., Burgess, J. M., Preece, R. D., et al. 2012, ApJS, 199, 19
Hotokezaka, K., Kyutoku, K., Okawa, H., Shibata, M., & Kiuchi, K. 2011, PhRvD, 83, 124008
Kiuchi, K., Sekiguchi, Y., Shibata, M., & Taniguchi, K. 2009, PhRvD, 80, 064037
Lee, W. H., Ramirez-Ruiz, E., & Granot, J. 2005, ApJL, 630, 165
McKinney, J. C., Tchekhovskoy, A., & Blandford, R. D. 2012, MNRAS, 423, 3083
McWilliams, S. T., & Levin, J. 2011, ApJ, 742, 90
Nava, L., Ghirlanda, G., Ghisellini, G., & Celotti, A. 2011, A&A, 530, A21
Nicuesa Guelbenzu, A., Klose, S., Greiner, J., et al. 2012, A&A, 548, A101
Norris, J. P., Gehrels, N., & Scargle, J. D. 2011, ApJ, 735, 23
Oechslin, R., & Janka, H.-T. 2006, MNRAS, 368, 1489
O'Shaughnessy, R., Belczynski, K., & Kalogera, V. 2008, ApJ, 675, 566
Paczynski, B. 1986, ApJL, 308, 43
Pannarale, F., Tonita, A., & Rezzolla, L. 2011, ApJ, 727, 95
Perna, R., & Belczynski, K. 2002, ApJ, 570, 252
Rezzolla, L., Baiotti, L., Giacomazzo, B., Link, D., & Font, J. A. 2010, CQGra, 27, 114105
Rezzolla, L., Giacomazzo, B., Baiotti, L., et al. 2011, ApJL, 732, 6
Sakamoto, T., Barthelmy, S. D., Baumgartner, W. H., et al. 2011, ApJS, 195, 2
Steiner, A. W., Lattimer, J. M., & Brown, E. F. 2012, arXiv:1205.6871
Tchekhovskoy, A., McKinney, J. C., & Narayan, R. 2012, JPhCS, 372, 012040
Tchekhovskoy, A., Narayan, R., & McKinney, J. C. 2011, MNRAS, 418, L79
Zhang, B., Liang, E., Page, K. L., et al. 2007, ApJ, 655, 989
Zhang, B., Zhang, B.-B., Virgili, F. J., et al. 2009, ApJ, 703, 1696